Final report for AOARD project FA23860914084: Fabrication of metamaterials by drawing techniques

Boris Kuhlmey, Simon Fleming, Alessandro Tuniz

Title: Fabrication of metamaterials by drawing techniques

Background: While metamaterials enable unprecedented control over propagation of light with applications such as lenses beating the diffraction limit for hyperfine imaging and lithography, fabrication of metamaterials for the optical regime is extremely difficult, as highly structured, repetitive metallic features at the nanoscale are required. The main barrier to experimental realization of optical metamaterials is the great difficulty of fabricating on this scale. Approaches divide into two main classes. Bottom-up approaches include molecular self-assembly and self-ordering. Whilst having the advantage of self-assembly, the structures are, as a result, typically quite limited as it is difficult to introduce spatial variations required for most devices. Top-down approaches such as e-beam or focused ion beam lithography can readily produce complex structures, however they have to individually create every part of the structure, which is a time consuming use of extremely expensive equipment, and limited to shallow, mostly 2D, structures. No existing technology is suitable to produce materials structured at nanoscopic scales in bulk.

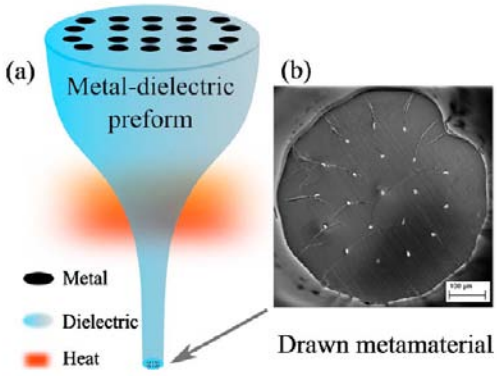

Figure 1: Princinple of the drawing technique

Vision: This project's vision is to create a novel and practical nanofabrication technique for metamaterials for frequencies ranging from the far infrared to visible light. This technique will make inexpensive volume production of metamaterials possible for the first time, It will do this by extending drawing, the technology used for making optical fiber, to preforms containing both metals and dielectrics.

Results Summary: Concentrating on the more accessible THz spectrum**,** we have demonstrated that the technique is viable, by fabricating and characterizing both electric [1] and magnetic metamaterials, including materials with measured negative permittivity [2,3]. The electric metamaterials are made by drawing polymer preforms containing indium wires (Figure 1), and we were able to experimentally demonstrate that this arrangement behaves as plasmonic materials with plasma frequency in the Thz spectrum [1]. Magnetic materials are more challenging to fabricate

Report Documentation Page

Form Approved
OMB No. 0704-0188

1. REPORT DATE	2. REPORT TYPE	3. DATES COVERED
03 MAR 2011	**FInal**	**22-07-2009 to 22-01-2011**

4. TITLE AND SUBTITLE
Fabrication of metamaterials by drawing techniques

5a. CONTRACT NUMBER
FA23860914084

5b. GRANT NUMBER

5c. PROGRAM ELEMENT NUMBER

6. AUTHOR(S)
Boris Kuhlmey

5d. PROJECT NUMBER

5e. TASK NUMBER

5f. WORK UNIT NUMBER

7. PERFORMING ORGANIZATION NAME(S) AND ADDRESS(ES)
University of Sydney,A28 Physics Road,Camperdown NSW 2006,Australia,AU,2006

8. PERFORMING ORGANIZATION REPORT NUMBER
N/A

9. SPONSORING/MONITORING AGENCY NAME(S) AND ADDRESS(ES)
AOARD, UNIT 45002, APO, AP, 96337-5002

10. SPONSOR/MONITOR'S ACRONYM(S)
AOARD

11. SPONSOR/MONITOR'S REPORT NUMBER(S)
AOARD-094084

12. DISTRIBUTION/AVAILABILITY STATEMENT
Approved for public release; distribution unlimited

13. SUPPLEMENTARY NOTES

14. ABSTRACT
This project researches the creation of novel and practical nanofabrication techniques for metamaterials operating at frequencies ranging from the far infrared to visible light. These techniques will make inexpensive volume production of metamaterials possible for the first time. It will do this by extending drawing, the technology used for making optical fiber, to preforms containing both metals and dielectrics.

15. SUBJECT TERMS
meta materials, fiber

16. SECURITY CLASSIFICATION OF:			17. LIMITATION OF ABSTRACT	18. NUMBER OF PAGES	19a. NAME OF RESPONSIBLE PERSON
a. REPORT	b. ABSTRACT	c. THIS PAGE			
unclassified	**unclassified**	**unclassified**	**Same as Report (SAR)**	**23**	

as they require non-circular metallic wires, which we were able to produce using two separate method. The first method on which we worked in collaboration with our colleague M. Large, was to draw a pure dielectric fiber and after drawing sputter the fiber with silver from one side, creating split ring resonators (Figure 2). We measured that these fibres have a magnetic resonance in the Thz, resulting in negative relative permeability [2,3].

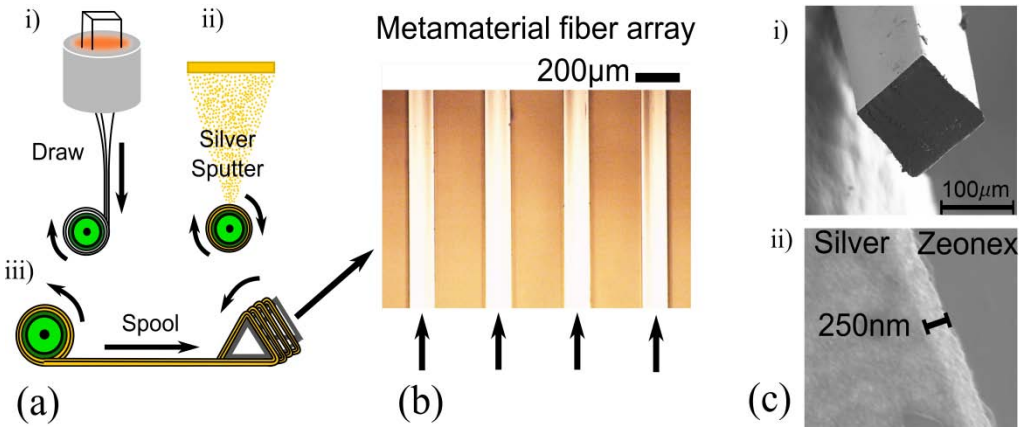

Figure 2: Fabrication of magnetic fiber metamaterial through sputtering. The silver coating is on three sides of the rectangular fiber only.

The second method was to create a non-circular indium shape within a polymer preform and draw this preform into a fiber. Figure 3 shows a resulting fiber, which also demonstrated a magnetic resonance in the THz (right panel of Fig. 3 shows the enhanced and phase shifted magnetic field at resonance [3,4]. At the time of writing we are exploring advanced drawing techniques suing multiple polymers to improve the shape of the magnetic resonators, with extremely promising results that indicate high quality magnetic resonators should be feasible also for the infrared spectrum.

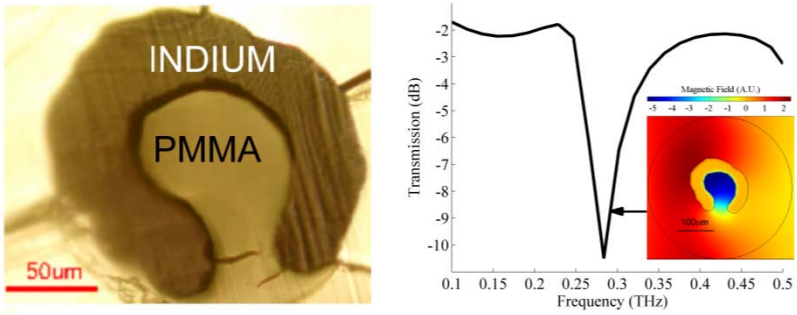

Figure 3: Direct drawn magnetic resonator (left); transmission of an array of the fiber and magnetic field at resonance (right).

We have experimentally demonstrated that the technique can draw materials with feature sizes well below the micron [4], paving the way to mid-infrared and visible metamaterials. We have numerically demonstrated that this technique will enable the fabrication of intrinsically invisible fibres [5,6], by creating composite materials that have the same refractive index as air (Figure 4).

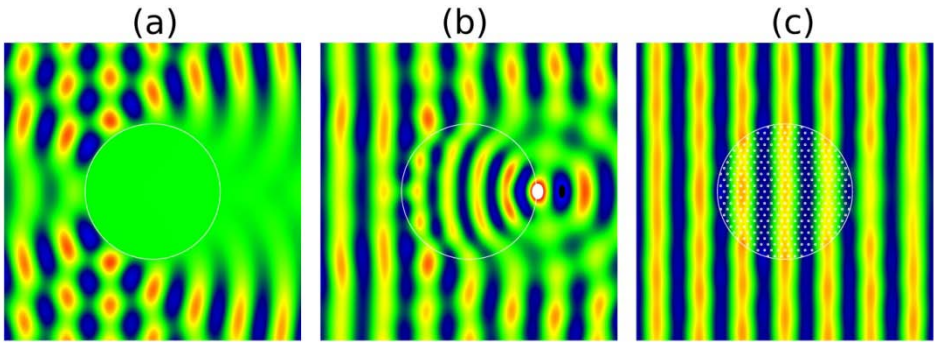

Figure 4: Electric field propagating around (a) a silver wire, (b) a glass fiber (c) a glass/silver nano-composite, all of same size, at a wavelength of 633nm (red light). The wave fronts are unaffected by the composite fiber, demonstrating the fiber is effectively invisible (scattering cross section reduction of more than 95%).

Future Work: There are two main directions for future work. The first is to make larger more complex structures on the current scale and use these to realize practical devices. The second is to make smaller scale structures for use in the IR and visible spectral regions.

Conclusion: The project has been extremely successful, demonstrating the feasibility of this novel technique for the practical fabrication of metamaterials. Having demonstrated the feasibility for simple structures at THz wavelengths, it opens up the possibility of practical metamaterial devices in the THz, and at shorter wavelengths.

Publications:

1. Tuniz, B. T. Kuhlmey, R. Lwin, A. Wang, J Anthony, R. Leonhardt, S.C. Fleming "Drawn metamaterials with plasmonic response at terahertz frequencies," ***Applied Physics Letters*** 96, article 191101 (2010)
2. A.Wang, A. Tuniz, P.G. Hunt, E.M. Pogson, R.A. Lewis, A. Bendavid, S.C. Fleming, B.T. Kuhlmey and M.C. J. Large, "Fiber metamaterials with negative magnetic permeability in the terahertz," ***Optics Materials Express***, in press: accepted 19/02/2011 (2011).
3. Alessandro Tuniz, Boris T. Kuhlmey, Anna Wang, Maryanne C. Large and Simon C. Fleming "Drawn Terahertz Metamaterials," Ninth International Conference on Photonic and Electromagnetic Crystal Structures (PECS), Grenada, Spain
4. Maryanne Large, Anna Wang, Peter Hunt, Alessandro Tuniz, Boris T. Kuhlmey, Simon C. Fleming, Elise Pogson, Roger Lewis, and Avi Bendavid, "Towards Woven Metamaterials for the THz", Photonics 2010, Indian Institute of Technology Guwahati, India, December 11-15, 2010 ***(invited talk)***
5. A. Tuniz, B. T. Kuhlmey, P.Y. Chen, S.C. Fleming, "Weaving the invisible thread: design of an optically invisible metamaterial fibre," ***Optics Express*** 18, pp. 18095-18105, (2010) *Prize for best student presentation*
6. A. Tuniz, B. T. Kuhlmey, P.Y. Chen, S.C. Fleming, "Design of an Optically Invisible Metamaterial Fibre," Australian Conference on Optical Fibre Technology (ACOFT), Melbourne, December 2010.

Detailed results can be found in the attached publications.

Drawn metamaterials with plasmonic response at terahertz frequencies

A. Tuniz,[1,a)] B. T. Kuhlmey,[1] R. Lwin,[1] A. Wang,[1] J. Anthony,[2] R. Leonhardt,[2] and S. C. Fleming[1]
[1]*Institute of Photonics and Optical Science (IPOS), School of Physics, University of Sydney, New South Wales 2006, Australia*
[2]*Department of Physics, University of Auckland, Private Bag 92019, Auckland, New Zealand*

(Received 16 March 2010; accepted 16 April 2010; published online 10 May 2010)

Electromagnetic metamaterials attract much attention since they can be engineered to exhibit optical properties not found in nature. Their fabrication, however, is challenging, especially in volume. We introduce drawing as a means of fabricating metamaterials, thus demonstrating a terahertz metamaterial. We codraw polymethyl-methacrylate and indium, producing several meters of metamaterial with wire diameters down to ~10 μm, and lattice constants of ~100 μm. We experimentally characterize the transmission properties of different samples, observing high-pass filtering between 0.3–0.4 THz, in good agreement with simulations. © *2010 American Institute of Physics*. [doi:10.1063/1.3428576]

Metamaterials hold great promise since they can be engineered to exhibit electromagnetic properties which are not found in nature, by tailoring their subwavelength structure. Recent demonstrations of exotic structures using metamaterials include electromagnetic cloaks,[1] negative refractive index media,[2] and sub-diffraction limited lenses.[3] Such devices, however, are challenging to fabricate, especially in large volumes. In this paper we report an example of a drawn metamaterial which has potential for inexpensive volume production. We produce more than 20 m of metamaterial in the form of a terahertz (THz) high-pass filter, with potential applications in THz imaging[4] and thermal detection.[5]

The electric response of our metamaterial is tailored via a two-dimensional array of thin metallic wires with subwavelength diameter and pitch. Most bulk metals have plasma frequencies in the visible and ultraviolet. However, a two-dimensional metallic wire array of diameter d and separation a in a dielectric with permittivity ϵ_d and refractive index n_d, irradiated by an electromagnetic field with the electric component parallel to the wires, can be seen as a metamaterial with lowered effective plasma frequency f_p such that

$$f_p^2 = \frac{(c_0/n_d)^2}{2\pi A_{\text{cell}}[\ln a^2/d(2a-d)]}, \tag{1}$$

where c_0 is the speed of light in vacuum and A_{cell} is the average area per wire of the metamaterial.[6] The permittivity as a function of frequency f is then given by

$$\epsilon_{\text{eff}}(f) = \epsilon_d\left(1 - \frac{f_p^2}{f^2 + 2i\gamma f}\right), \tag{2}$$

where γ is a damping factor.[6] This equation describes the effective medium's transition from metal-like behavior (low transmission due to negative permittivity), to dielectric-like behavior (higher transmission due to positive permittivity). Arrays of thin metallic wires are thus metamaterial high-pass filters in the vicinity of the plasma frequency f_p.

The fabrication of metamaterials operating at frequencies higher than the microwave remains challenging, often relying on expensive lithographic techniques which can only be used up to centimeter scales.[7] We present a fabrication approach inspired by fiber drawing[8] used for the large scale and accurate fabrication of photonic crystal fibers (PCFs). Figure 1(a) shows a schematic of how our metamaterials are drawn; a macroscopically sized metal-dielectric preform is heated and reduced in size by several orders of magnitude. However, there are additional fabrication challenges when compared to conventional PCFs; the scales required are typically smaller ($\lesssim$200 nm for optical metamaterials), and being metal-dielectric structures, material properties (such as viscosity and melting temperature) are not well matched. In spite of this, many meters of microstructured copper-silica fibers were recently drawn for the purpose of demonstrating guided modes via metallic reflection.[9] Similar structures have been achieved by pumping liquid metals into already drawn holey PCFs with submicrometer holes,[10] however direct pumping is limited by pressure to fabricating samples a few meters in length at most, while direct drawing can in principle be scaled to kilometer lengths.

Here we present the fabrication of drawn metamaterials, comprised of microstructured indium-filled polymethyl-methacrylate (PMMA) fiber, exhibiting plasmonic response in the THz. Indium wires below ~10 μm diameter and ~100 μm separation are achieved, though submicron features are possible.[10] We show that the plasmonic response

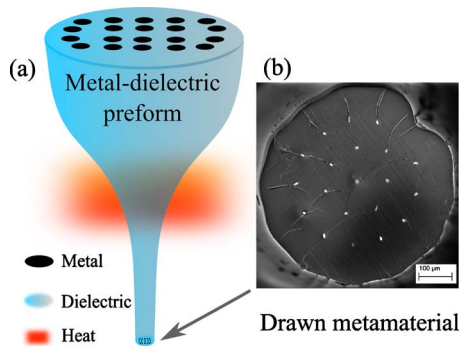

FIG. 1. (Color online) (a) Schematic of a metal-dielectric preform, drawn into a metamaterial via heating. (b) SEM micrograph of a fabricated 590 μm indium-filled PMMA fiber cross-section.

[a)]Electronic mail: alessandro.tuniz@sydney.edu.au.

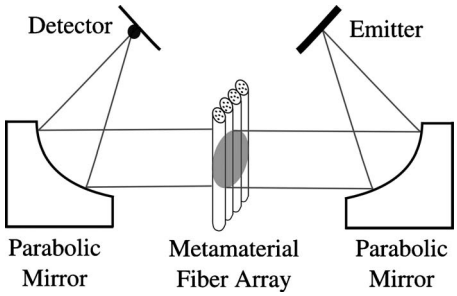

FIG. 2. Schematic of the experimental setup for measuring metamaterial fiber transmittance.

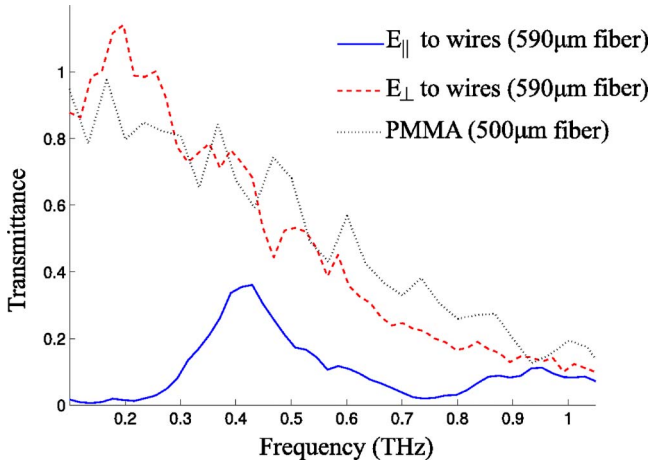

FIG. 3. (Color online) Experimentally measured metamaterial transmittance, normalized to transmission through aperture only. The electric field E is either parallel (solid line) or perpendicular (dashed line) to the wires. A measurement for an array of 500 μm PMMA fibers is also shown (dotted line).

can be controlled via the drawing speed, and compare results with numerical simulations.

Our fabrication procedure is based on adapting the Taylor-wire process[11] to indium wires in PMMA tubes, in combination with the stack-and-draw procedure used for fabricating PCFs. PMMA was chosen because it is an easily machined and drawn dielectric; indium because it has the appropriate melting temperature (156.6 °C) for codrawing with PMMA. Together their properties are suitable for the THz region. The metamaterial fabrication procedure was as follows. We included an indium wire (1 mm diameter, 99.99% purity) in a PMMA tube with 1.2 mm inside diameter (ID) and 12 mm outside diameter (OD), sealed at one end. The tube was evacuated and drawn down at a temperature of 185 °C to an outer diameter of 1.2 mm. The resulting fiber was then cut into smaller pieces, which were stacked in a PMMA capillary (6.0 mm ID, 7.5 mm OD). This stack was sealed at one end and fed into a furnace while being rapidly drawn, reducing the diameter of the structure by a factor of 10, and increasing the length by a factor of 100. By varying the draw speed, we fabricated fibers with diameters of 590, 690, and 770 μm. The metal wires' diameters and their separation scaled down correspondingly. Figure 1(b) shows a scanning electron microscope (SEM) image of a 590 μm indium-filled metamaterial fiber cross section. The wires have a lattice constant $a \sim 100$ μm and diameter $d \sim 8$ μm.

We characterized the optical properties of our samples via THz time domain spectroscopy.[12] A schematic of the experimental setup is shown in Fig. 2. The THz source was an InGaAs surface emitter pumped by 80 fs, 800 nm pulses from a mode-locked Ti:Sapphire laser, while the detector was a photoconductive antenna which was gated by a time-delayed pulse from the same laser. The gated antenna current which is proportional to the incident THz electric field is measured with a lock-in amplifier. The entire THz transmission spectrum (between 0.1–1.1 THz) was obtained from the Fourier transform of the time-delay scans between pump and probe pulses. We cut the final fibers in many 3 cm pieces, aligned them in a one-dimensional array, and measured the transmittance for polarized light either parallel or perpendicular to the wires. The final sample sizes had areas of 3 $\times 3$ cm^2, and were attached to a metal plate with a circular aperture along the collimated THz beam. From repeated measurements we estimate a noise level in transmittance of about 10% for frequencies higher than 0.2 THz, and 20% for frequencies lower than 0.2 THz.

Figure 3 (blue solid line) shows the measured transmittance of our 590 μm fiber for wires parallel to the electric field E, where they form a metamaterial. Very good agreement is found with previous work.[13] We observe that transmission is extremely small at low frequencies, up to a transition region at ~0.3 THz. At higher frequencies the sample behaves like a dielectric until the wavelength becomes too short and our structure can no longer be seen as a homogeneous medium, as discussed in detail below.

The dashed red line in Fig. 3 shows the measured transmittance when the wires are perpendicular to E. In this case, Eqs. (1) and (2) do not apply, and the transmittance is close to that of an array of 500 μm pure PMMA fibers (black dotted line). Thus, our system is both a polarizer and a high-pass filter metamaterial.

To study the ability to engineer plasmonic responses by varying the draw speed, we measured the transmittance of arrays of different fiber diameters, with E parallel to the wires. The results are shown in Fig. 4(a). The plasmonic transition region shifts to lower frequencies as we increase the fiber diameter, since the wires' separation a and diameter d scale correspondingly, leading to a decrease in the plasma frequency of the wire array, c.f. Eq. (1). We modeled the transmittance using the finite element package COMSOL, mapping the microstructured geometries and wire diameters obtained from SEM images, and using PMMA refractive index[14,15] and indium permittivity[16] [Fig. 4(b)], observing good agreement with the experiment. Note that Eq. (1) predicts plasma frequencies of 0.59 THz, 0.50 THz, and 0.45 THz for the 590 μm, 690 μm, and 770 μm fibers, respectively, assuming $A_{\text{cell}} = \sqrt{3}a^2/2$. Figure 4(a) shows that the measured transmission peaks below such values. This is due to the PMMA jacket that surrounds the metamaterial present at the fiber core. To illustrate this, we simulate the transmittance of homogeneous metamaterials with plasma frequencies f_p predicted by Eq. (1), possessing permittivity described by Eq. (2), surrounded by a PMMA jacket [Fig. 4(c)]. Figures 4(b) and 4(c) are in excellent agreement at low frequencies (white background), where the wavelength is much larger than any feature of the wire array. Some discrepancies appear at higher frequencies, when the structure's features are no longer small compared to the wavelength (shaded region): at these frequencies Bragg scattering and other resonant phenomena due to details of the structure can

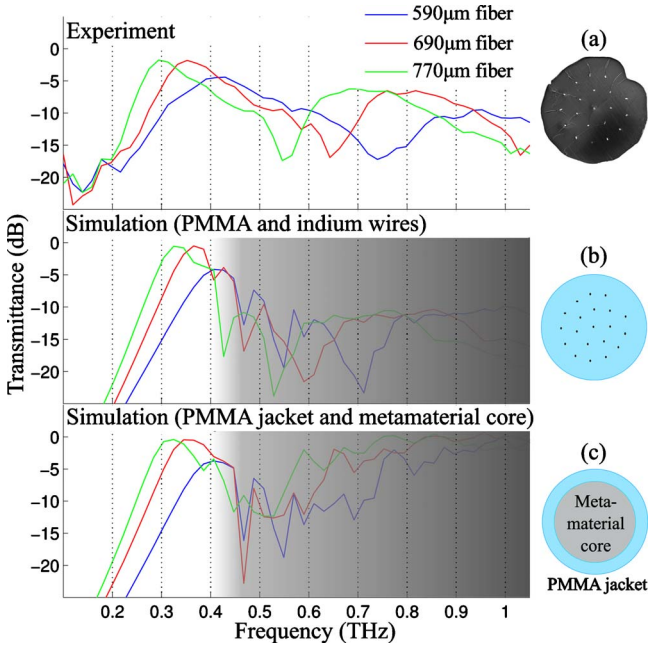

FIG. 4. (Color online) (a) Experimental and (b) simulated transmittance for different arrays of metamaterial fiber. (c) Simulated transmittance for metamaterials surrounded by a PMMA jacket. The electric field is parallel to the wires. The shaded region illustrates where the medium cannot be seen as homogeneous.

alter the transmission, and the array can no longer be considered as a homogeneous medium. The shaded region is to aid the eye and does not represent a theoretical value at which the medium ceases to be homogeneous.

Note that a similar metamaterial was fabricated some years ago using microstereolithography.[13] While such a structure was only of the order of a few millimeters in size, we were able to inexpensively fabricate many meters of a similar geometry through drawing. Our technique potentially allows to fabricate kilometers of continuous metamaterial with feature sizes down to the nanoscale, moving device operating frequencies into the mid-infrared and visible. Such fiber-shaped metamaterials can be cut and stacked into bulk materials to realize a large number of devices, or woven into more complex structures. This could open the way to fabricating cost-effective plasmonic devices and optical metamaterials on a mass scale, though in this frequency range using low loss metals and dielectrics, such as silver and silica, would be preferable.

In conclusion, we have demonstrated drawn metamaterials that act as THz high-pass filters and polarizers. Transmittance was measured via THz time domain spectroscopy, finding good agreement with numerical simulations. Finally, we have introduced drawing as a means of mass-producing metamaterials. An extension of this procedure would reduce metal features down to the nanoscale, potentially leading to low-cost optical metamaterial and plasmonic devices.

This work was performed in part at the Optofab node of the Australian National Fabrication Facility using Commonwealth and NSW State Government funding. This material is based on research sponsored by the Air Force Research Laboratory, under Agreement No. FA2386-09-1-4084. B.T.K. acknowledges support from an Australian Research Council Future Fellowship.

[1]D. Schurig, J. J. Mock, B. J. Justice, S. A. Cummer, J. B. Pendry, A. F. Starr, and D. R. Smith, Science **314**, 977 (2006).
[2]V. M. Shalaev, Nat. Photonics **1**, 41 (2007).
[3]Z. Liu, H. Lee, Y. Xiong, C. Sun, and X. Zhang, Science **315**, 1686 (2007).
[4]V. M. Lubecke, K. Mizuno, and G. M. Rebeiz, IEEE Trans. Microwave Theory Tech. **46**, 1821 (1998).
[5]M. A. Tarasov, V. D. Gromov, G. D. Bogomolov, E. A. Otto, and L. S. Kuzmin, Instrum. Exp. Tech. **52**, 74 (2009).
[6]S. I. Maslovski and M. G. Silveirinha, Phys. Rev. B **80**, 245101 (2009).
[7]A. Boltasseva and V. M. Shalaev, Metamaterials **2**, 1 (2008).
[8]J. C. Knight, Nature (London) **424**, 847 (2003).
[9]J. Hou, D. Bird, A. George, S. Maier, B. T. Kuhlmey, and J. C. Knight, Opt. Express **16**, 5983 (2008).
[10]M. A. Schmidt, L. N. Prill Sempere, H. K. Tyagi, C. G. Poulton, and P. S. J. Russell, Phys. Rev. B **77**, 033417 (2008).
[11]I. W. Donald and B. L. Metcalfe, J. Mater. Sci. **31**, 1139 (1996).
[12]Y. H. Lo and R. Leonhardt, Opt. Express **16**, 15991 (2008).
[13]D. Wu, N. Fang, C. Sun, X. Zhang, W. J. Padilla, D. N. Basov, D. R. Smith, and S. Schultz, Appl. Phys. Lett. **83**, 201 (2003).
[14]Y. S. Jin, G. J. Kim, and S. G. Jeon, J. Korean Phys. Soc. **49**, 513 (2006).
[15]M. Lee, O. Mitrofanov, H. E. Katz, and C. Erben, Appl. Phys. Lett. **81**, 1474 (2002).
[16]R. Y. Koyama, N. V. Smith, and W. E. Spicer, Phys. Rev. B **8**, 2426 (1973).

Weaving the invisible thread: design of an optically invisible metamaterial fibre

Alessandro Tuniz,* Boris T. Kuhlmey, Parry Y. Chen and Simon C. Fleming

Institute of Photonics and Optical Science (IPOS), School of Physics, University of Sydney, New South Wales 2006, Australia

**alessandro.tuniz@sydney.edu.au*

Abstract: We present the design of an invisible metamaterial fibre operating at optical frequencies, which could be fabricated by adapting existing fibre drawing techniques. The invisibility is realised by matching the refractive index of the metamaterial fibre with the surroundings. We present a general recipe for the fabrication of such fibres, and numerically characterise a specific example using hexagonally arranged silver nanowires in a silica background. We find that invisibility is highly sensitive to details of the metamaterial boundary, a problem that is likely to affect most invisibility and cloaking schemes.

OCIS codes: (060.2400) Fiber properties; (160.3918) Metamaterials; (290.5893) Scattering, invisibility.

References and links

1. J. Ward, "Towards invisible glass," Vacuum **22**(9), 369–375 (1972).
2. R. L. Fante, M. T. McCormack, T. D. Syst, and M. A. Wilmington, "Reflection properties of the Salisbury screen," IEEE Trans. Antenn. Propag. **36**(10), 1443–1454 (1988).
3. A. Alù, and N. Engheta, "Achieving transparency with plasmonic and metamaterial coatings," Phys. Rev. E Stat. Nonlin. Soft Matter Phys. **72**(1), 016623 (2005).
4. A. Alù, and N. Engheta, "Plasmonic materials in transparency and cloaking problems: mechanism, robustness, and physical insights," Opt. Express **15**(6), 3318–3332 (2007).
5. B. Edwards, A. Alù, M. G. Silveirinha, and N. Engheta, "Experimental verification of plasmonic cloaking at microwave frequencies with metamaterials," Phys. Rev. Lett. **103**(15), 153901 (2009).
6. J. B. Pendry, D. Schurig, and D. R. Smith, "Controlling electromagnetic fields," Science **312**(5781), 1780–1782 (2006).
7. D. Schurig, J. J. Mock, B. J. Justice, S. A. Cummer, J. B. Pendry, A. F. Starr, and D. R. Smith, "Metamaterial electromagnetic cloak at microwave frequencies," Science **314**(5801), 977–980 (2006).
8. J. Valentine, J. Li, T. Zentgraf, G. Bartal, and X. Zhang, "An optical cloak made of dielectrics," Nat. Mater. **8**(7), 568–571 (2009).
9. T. Ergin, N. Stenger, P. Brenner, J. B. Pendry, and M. Wegener, "Three-dimensional invisibility cloak at optical wavelengths," Science **328**(5976), 337–339 (2010).
10. N. A. Nicorovici, G. W. Milton, R. C. McPhedran, and L. C. Botten, "Quasistatic cloaking of two-dimensional polarizable discrete systems by anomalous resonance," Opt. Express **15**(10), 6314–6323 (2007).
11. W.-H. Sun, Y. Lu, R.-W. Peng, L.-S. Cao, D. Li, X. Wu, and M. Wang, "Omnidirectional transparency induced by matched impedance in disordered metamaterials," J. Appl. Phys. **106**(1), 013104 (2009).
12. Y. Fang, and S. He, "Transparent structure consisting of metamaterial layers and matching layers," Phys. Rev. A **78**(2), 023813 (2008).
13. C. Yang, J. Yang, M. Huang, J. Shi, and J. Peng, "Electromagnetic cylindrical transparent devices with irregular cross section," Radioengineering **19**, 136–140 (2010).
14. J. Hou, D. Bird, A. George, S. Maier, B. T. Kuhlmey, and J. C. Knight, "Metallic mode confinement in microstructured fibres," Opt. Express **16**(9), 5983–5990 (2008).
15. A. Tuniz, B. T. Kuhlmey, R. Lwin, A. Wang, J. Anthony, R. Leonhardt, and S. C. Fleming, "Drawn metamaterials with plasmonic response at terahertz frequencies," Appl. Phys. Lett. **96**(19), 191101 (2010).
16. M. A. Schmidt, L. N. Prill Sempere, H. K. Tyagi, C. G. Poulton, and P. S. J. Russell, "Waveguiding and plasmon resonances in two-dimensional photonic lattices of gold and silver nanowires," Phys. Rev. B **77**(3), 033417 (2008).
17. Y. Ruan, H. Ebendorff-Heidepriem, and T. M. Monro, "Subwavelength soft glass fibres with extremely small hole size for field enhancement," in *Proceedings of the Australasian Conference on Optics, Lasers and Spectroscopy and Australian Conference on Optical Fibre Technology* (Adelaide, Australia, 2009).
18. J. C. Knight, "Photonic crystal fibres," Nature **424**(6950), 847–851 (2003).
19. A. Boltasseva, and V. M. Shalaev, "Fabrication of optical negative-index metamaterials: recent advances and outlook," Metamaterials (Amst.) **2**(1), 1–17 (2008).

#130951 - $15.00 USD Received 30 Jun 2010; revised 4 Aug 2010; accepted 5 Aug 2010; published 6 Aug 2010

20. M. Yan, and N. A. Mortensen, "Hollow-core infrared fiber incorporating metal-wire metamaterial," Opt. Express **17**(17), 14851–14864 (2009).
21. E. J. Smith, Z. Liu, Y. Mei, and O. G. Schmidt, "Combined surface plasmon and classical waveguiding through metamaterial fiber design," Nano Lett. **10**(1), 1–5 (2010).
22. A. Tuniz, P. Chen, B. T. Kuhlmey, and S. C. Fleming, "Design of an optical hyperlens with metallic nanocylinders," in *Proceedings of META '10, 2nd International Conference on Metamaterials, Photonc Crystals and Plasmonics* (Cairo, Egypt, 2010).
23. P. Markos, and C. M. Soukoulis, *Wave Propagation: From Electrons to Photonic Crystals and Left-Handed Materials* (Princeton University Press, 2008), Chap. 14.
24. R. C. McPhedran, N. A. Nicorovici, and L. C. Botten, "The TEM mode and homogenization of doubly periodic structures," J. Electromagn. Waves Appl. **11**(7), 981–1012 (1997).
25. P. B. Johnson, and R. W. Christy, "Optical constants of the noble metals," Phys. Rev. B **6**(12), 4370–4379 (1972).
26. I. H. Malitson, "Interspecimen Comparison of the Refractive Index of Fused Silica," J. Opt. Soc. Am. **55**(10), 1205–1208 (1965).
27. R. C. McPhedran, C. G. Poulton, N. A. Nicorovici, and A. B. Movchan, "Low frequency corrections to the static effective dielectric constant of a two-dimensional composite material," Proc. R. Soc. Lond. A **452**(1953), 2231–2245 (1996).
28. L. C. Botten, N. A. P. Nicorovici, A. A. Asatryan, R. C. McPhedran, C. M. de Sterke, and P. A. Robinson, "Formulation for electromagnetic scattering and propagation through grating stacks of metallic and dielectric cylinders for photonic crystal calculations. Part I. Method," J. Opt. Soc. Am. A **17**(12), 2165–2176 (2000).
29. R. C. McPhedran, N. A. Nicorovici, L. C. Botten, and K. A. Grubits, "Lattice sums for gratings and arrays," J. Math. Phys. **41**(11), 7808–7816 (2000).
30. T. P. White, B. T. Kuhlmey, R. C. McPhedran, D. Maystre, G. Renversez, C. M. De Sterke, and L. C. Botten, "Multipole method for microstructured optical fibers. I. Formulation," J. Opt. Soc. Am. B **19**(10), 2322–2330 (2002).
31. B. T. Kuhlmey, T. P. White, G. Renversez, D. Maystre, L. C. Botten, C. M. de Sterke, and R. C. McPhedran, "Multipole method for microstructured optical fibers. II. Implementation and results," J. Opt. Soc. Am. B **19**(10), 2331–2340 (2002).
32. D. Felbacq, G. Tayeb, and D. Maystre, "Scattering by a random set of parallel cylinders," J. Opt. Soc. Am. A **11**(9), 2526–2538 (1994).
33. P. S. Kildal, A. A. Kishk, and A. Tengs, "Reduction of forward scattering from cylindrical objects using hardsurfaces," IEEE Trans. Antenn. Propag. **44**(11), 1509–1520 (1996).
34. E. F. Knott, J. F. Shaeffer, and M. T. Tuley, *Radar cross section* (New York: SciTech Publishing, 2004), Chapter 3.

1. Introduction

Electromagnetic invisibility, i.e. the passing of light through a structure without scattering, distortion, or absorption, is currently of great interest, due to its fascinating implications. A number of structures that are invisible to electromagnetic radiation have been theoretically proposed and experimentally demonstrated in the past few years; from simple devices such as antireflection coatings [1] and absorbing screens [2], to more exotic structures such electromagnetic cloaks, which can hide an object with a plasmonic medium [3–5] or a metamaterial possessing especially engineered effective optical properties [6–10]. In this paper we discuss metamaterials that are themselves optically transparent, as opposed to possessing cloaking properties. Recent proposals of transparent metamaterials are based on alternating layers of natural materials and double-negative metamaterials [11,12] and transformation optics [13].

Here we propose a much simpler approach: optical transparency is achieved by designing a metamaterial with refractive index that matches the surroundings, consisting of an array of sub-wavelength metallic nanocylinders surrounded by a dielectric. Such structures could potentially be fabricated via metamaterial fibre drawing, either via direct co-drawing, in which a macroscopically sized metal-dielectric preform is heated and reduced in size by several orders of magnitude [14,15], or via pumping liquid metal into existing micro- and nano- structured holey photonic crystal fibres (PCFs) [16]. Holey fibres containing feature

#130951 - $15.00 USD Received 30 Jun 2010; revised 4 Aug 2010; accepted 5 Aug 2010; published 6 Aug 2010

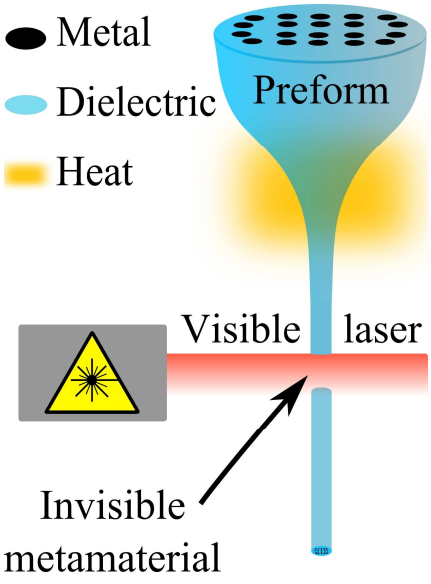

Fig. 1. Schematic of a metal-dielectric preform, drawn into a metamaterial via heating, designed to be invisible at a chosen optical wavelength (e.g. 633nm).

sizes down to 30nm have recently been reported [17], showing that drawn patterned nanostructures, and thus drawn optical metamaterials, can in principle be produced.

Fibre drawing has already proven extremely successful for the large scale and accurate fabrication of PCFs [18]. In the context of metamaterials, drawing has significant advantages over conventional fabrication techniques, especially in terms of cost (the macroscopic preform is generally an inexpensive dielectric a few cm^3 in volume) and volume production (one preform can in principle be used to make kilometers of fibre). In contrast, the lithographic techniques used for producing metamaterials at operating frequencies from the terahertz to the visible are generally quite expensive, and produce no more than a few cm^2 of metamaterial at a time [19]. However, while drawing offers the possibility of creating nanoscale structures in volume, this comes with a constraint – they have to be uniform along one dimension. Recently it has been shown that important functionality can potentially be realised with such fibre-based metamaterials, such as low-loss mid-IR waveguiding [20], sub-wavelength waveguiding [21] and hyperlensing [22].

Here we propose another interesting structure that can be fabricated via drawing of metal cylinders in a dielectric – the optically invisible fibre. Figure 1 illustrates a schematic of the potential fabrication process, whereby a macroscopic metal-dielectric preform is drawn into a fibre that is invisible around a chosen optical wavelength (e.g. λ = 633nm for a He:Ne laser) with normal incidence. Our design method is based on matching the effective optical parameters for a metamaterial of 2-dimensional patterned nanocylinders of sub-wavelength pitch to its surroundings. We characterise our invisible fibre via the total scattering cross section σ_T, showing that σ_T has a minimum when the real part of the metamaterial effective refractive index matches the surroundings. Taking the example of a fibre to be invisible at 633nm using silver nanocylinders in a silica cylinder of radius R = 1μm, we study the behaviour of σ_T with wavelength, incident angle, and polarisation. In this case more than a 95% reduction in σ_T can be achieved over ~13nm bandwidth when compared to dielectric and conducting cylinders of the same size, as well as a 95% reduction in σ_T for angles that are ± 10° to normal incidence at 633nm. We find that invisibility is highly sensitive to changes in the metamaterial boundary, with best results when the *total* filling fraction – including the metamaterial boundaries – matches the bulk filling fraction. Thus, particular attention should be paid to the fibre preform design process. At larger fibre diameters our invisible

#130951 - $15.00 USD Received 30 Jun 2010; revised 4 Aug 2010; accepted 5 Aug 2010; published 6 Aug 2010

metamaterial becomes a near-perfect absorber, due its low reflectance and inherently lossy nature.

2. Material design – bulk properties

2.1 Principle

An object in vacuum is invisible if it neither reflects nor absorbs light, and if it induces no changes in phase with respect to its surroundings. Our objective is to realise an optical metamaterial that closely meets such requirements.

The optical properties of a homogeneous material are commonly characterised via its complex impedance z and refractive index n, related to the relative electric permittivity $\varepsilon = n/z$ and relative magnetic permeability $\mu = nz$. The impedance mismatch at an interface causes reflections, while the refractive index characterises the phase velocity in the medium. For example, for a homogeneous slab of length L, the transmission and reflection coefficients t and r for a plane wave of angular frequency ω at normal incidence are given by [23]

$$t = \frac{1}{\cos\frac{n\omega L}{c} - \frac{i}{2}\left(z + \frac{1}{z}\right)\sin\frac{n\omega L}{c}}, \tag{1}$$

$$\frac{r}{t} = -\frac{i}{2}\left(z - \frac{1}{z}\right)\sin\frac{n\omega L}{c}, \tag{2}$$

where c is the speed of light in vacuum.

It goes without saying that a hypothetical slab with $n = 1$ and $z = 1$ is invisible in vacuum, since $r = 0$ and $t = \exp(i\omega L/c)$. Natural materials possess an impedance and refractive index that are not unity at optical wavelengths, and are thus visible; typically bulk metals possess a permittivity $\varepsilon_m < 0$ and dielectrics possess $\varepsilon_d > 1$, with $\mu = 1$ for both.

However, it is well known that a composite medium composed of a 2-dimensional array of thin metal wires surrounded by a dielectric in the electrostatic limit (feature sizes much smaller than the wavelength) irradiated by TE polarised light (electric field directed along the wires) can be treated as a homogeneous medium with effective permittivity ε_{eff} given by

$$\varepsilon_{eff} = f\varepsilon_m + (1-f)\varepsilon_d, \tag{3}$$

where f is the area filling fraction of the metal (see, for example, Ref [24].). Thus, by knowing ε_m and ε_d at a given wavelength, it is possible to compute the filling fraction at which the composite medium is invisible by solving for $\varepsilon_{eff} = 1$ in Eq. (3), yielding

$$f = \frac{1-\varepsilon_d}{\varepsilon_m - \varepsilon_d}. \tag{4}$$

Assuming for now that the composite medium is effectively non-magnetic ($\mu_{eff} = 1$), for f satisfying Eq. (4) the effective index and impedance take the values $n_{eff} = 1$ and $z_{eff} = 1$ respectively, as required.

By applying the above procedure at a wavelength λ = 633nm using silver ($\varepsilon_{Ag} = -17.7 + 0.49i$ from interpolated values of Ref [25].) and silica ($\varepsilon_{silica} = 2.123$ from the Sellmeier equation [26]), one obtains that $\varepsilon_{eff} = 1.00 + 0.03i$ when $f = 0.0567$. For a hexagonal lattice of cylinders with radius r and centre-to-centre pitch d, i.e. $f = \pi r^2/(\sqrt{3}d^2/2)$,

#130951 - $15.00 USD Received 30 Jun 2010; revised 4 Aug 2010; accepted 5 Aug 2010; published 6 Aug 2010

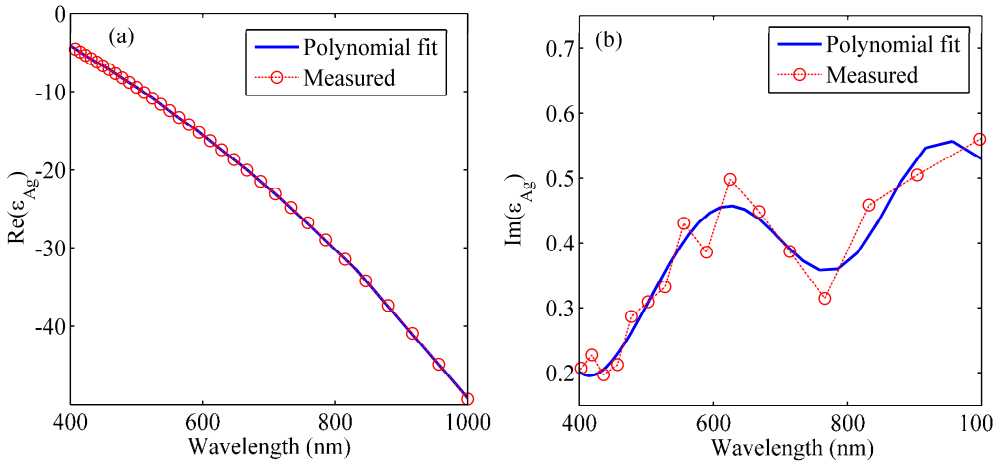

Fig. 2. (a) Real and (b) imaginary parts of the permittivity of silver at optical wavelengths: the blue solid line represents the polynomial fit used in the numerical model, the red markers indicate experimental values.

one finds that for a cylinder diameter of $2r$ = 30nm (the smallest drawn feature reported [17]), the pitch must be d = 120nm, in which case λ/d ~4 and the electrostatic approximation is not appropriate.

Thus, while Eq. (3) is a good starting point, higher order corrections [27] are necessary to achieve higher precision in calculating the filling fraction required for invisibility.

2.2 Higher order corrections

Here we obtain corrections to the first-order theory by directly calculating r and t and inverting Eqs. (1) and (2),

$$\cos\frac{n\omega L}{c} = \frac{1}{2t}[1-r^2+t^2], \tag{5}$$

$$z = \pm\sqrt{\frac{(1+r)^2-t^2}{(1-r)^2-t^2}}, \tag{6}$$

for different slabs of lengths $L = d, 2d, 3d$. Following the procedure outlined in [23], using Eq. (5) and (6) we verify that z is independent of L, and unambiguously retrieve n (and thus ε and μ) at a given wavelength.

We use a multipole expansion in combination with the transfer matrix method to calculate r and t for uniform slabs of hexagonally arranged silver cylinders in a silica background under TE polarisation. Fields around each cylinder are expanded in a multipole basis, where analytic expressions are derived for the cylindrical boundary conditions [28]. Lattice sums are used to relate the field incoming onto each cylinder to the field outgoing from other cylinders within a singer layer of the lattice [29]. The scattering and reflection coefficients of a multi-layer stack of gratings are computed from the coefficients of a single grating layer via a recurrence relation. The permittivity of silica is included in the calculations via a wavelength-dependent Sellmeier expansion [26], whereas for silver we use a ninth-order polynomial fit to measured real and imaginary parts of complex permittivity [25] [Fig. 2(a) and 2(b)].

We use this method to calculate r, t, and extract n, z, as a function of f for two fixed unit cell lengths, d = 10nm and d = 100nm. The results are shown in Fig. 3(a) and 3(b): whereas for smaller lattices (d = 10nm, i.e. λ/d ~60), calculations are in excellent agreement with the quasistatic theory of Eq. (3), for larger lattices (d = 100nm, i.e. λ/d ~6) a significant correction

#130951 - $15.00 USD Received 30 Jun 2010; revised 4 Aug 2010; accepted 5 Aug 2010; published 6 Aug 2010

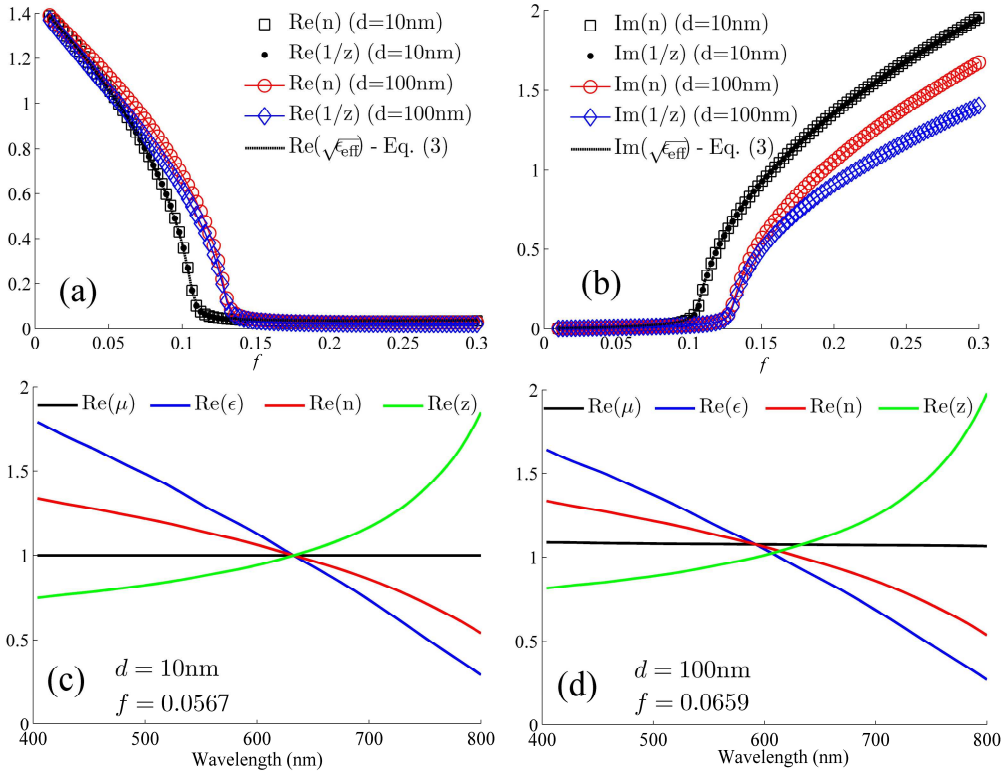

Fig. 3. (a) Real and (b) imaginary parts of effective refractive index and impedance as a function of filling fraction f for hexagonally arranged silver cylinders in a silica background at a wavelength of λ = 633nm, retrieved for d = 10nm and d = 100nm, and calculated through Eq. (3). Note that effective medium theory [Eq. (3)] applies only for smaller unit cells. (c) Real parts of retrieved effective optical parameters as a function of wavelength for d = 10nm, f = 0.0567 and (d) for d = 100nm, f = 0.0659. In both cases $Re(n)$ = 1 at 633nm by design, but for the larger unit cell size a magnetic response is present.

to the first order theory is required. Analytical work on the homogenisation of arrays of metallic cylinders [27] has shown that lowest order dynamic corrections to the static homogenisation theory lead to an additional dipolar magnetic response as well as a quadrupolar electric response, both of same order of magnitude. In particular, the combination of these two effects explains that we have $z \neq 1/n$.

From Fig. 3(b) we conclude that a filling fraction f = 0.0659 yields an effective index of 1.00 + 0.01i at λ = 633nm for a lattice constant of d = 100nm, corresponding to a cylinder diameter of 2r = 27nm, which can potentially be achieved using fibre drawing techniques.

Figures 3(c) and 3(d) shows the real parts of the optical parameters extracted as a function of wavelength for d = 10nm, f = 0.0567 and for d = 100nm, f = 0.0659. In the former case [Fig. 3(c)], all optical parameters are unity at 633nm by design. In the latter case [Fig. 3(d)], the presence of a magnetic response makes it impossible to simultaneously match the refractive index and the impedance to the surroundings. As we will see next, this does not compromise device performance at the desired wavelength. We now characterise its visibility in detail in a fibre geometry.

#130951 - $15.00 USD Received 30 Jun 2010; revised 4 Aug 2010; accepted 5 Aug 2010; published 6 Aug 2010

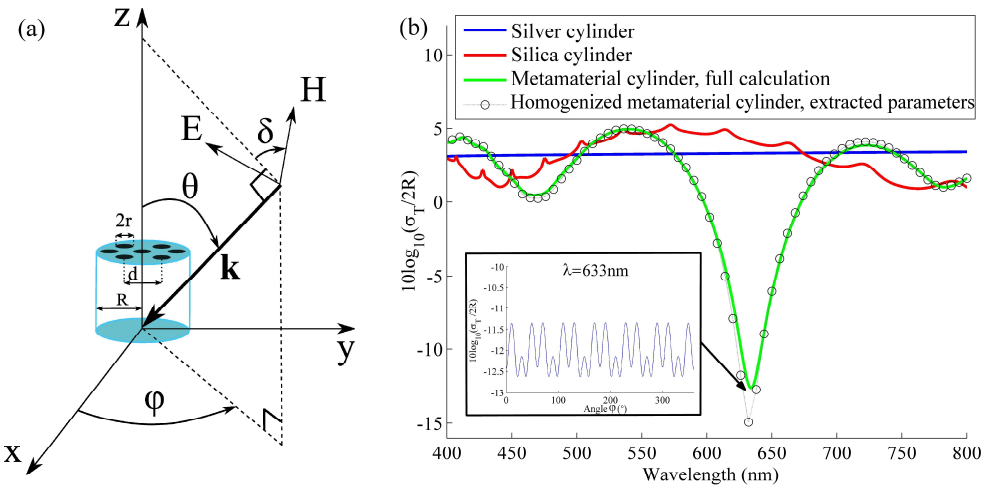

Fig. 4. (a) Schematic of incident wave parameters with respect to the axis of a dielectric cylinder with radius *R*, filled with hexagonally arranged metal nanocylinders of radius *r* and centre-to-centre pitch *d*. φ indicates azimuthal dependence, θ indicates the incident angle of the wave vector **k** with respect to the cylinder axis and δ indicates the angle of polarisation. (b) Normalised scattering cross section for different cylinders with R = 1μm. The designed metamaterial cylinder has a minimum cross section at the chosen wavelength of 633nm. Inset: Normalised scattering cross section (full calculation) for the metamaterial cylinder as a function of azimuthal angle.

3. Numerical simulations and analysis

We use the multipole method [30,31] to evaluate scattering of waves [32] at optical wavelengths for two-dimensional cylinders of radius R made out of the metamaterial characterised in Section 2.2. This method allows to characterise visibility via semi-analytical calculations of the scattering cross section (SCS) for any linear polarisation state, azimuthal angle, and incident angle with respect to the cylinder axis [represented by δ, φ and θ respectively, as shown in the schematic of Fig. 4(a)]. The scattering cross section σ is defined as the total scattered power per unit length at large distances, normalised to the incident power density. In polar coordinates (ρ,α) this is written as

$$\sigma(\alpha) = \lim_{\rho\to+\infty} 2\pi\rho \frac{\left|\mathbf{E}^S(\rho,\alpha)\right|^2}{\left|\mathbf{E}^0(\rho,\alpha)\right|^2}, \tag{7}$$

where $\mathbf{E^0}$ and $\mathbf{E^S}$ are the incident and scattered electric field, respectively. One then obtains the total SCS σ_T by integrating over all angles,

$$\sigma_T = \frac{1}{2\pi}\int_0^{2\pi} \sigma(\alpha) d\alpha\,. \tag{8}$$

Another parameter for characterising the scattering properties of objects is the equivalent blockage width W_{eq} a complex-valued parameter defined as the width of an ideal shadow which produces the same forward-scattered field as the cylinder being observed [33]. It can be shown that $\sigma_T = 2Re(W_{eq})$. It follows, for example, that at a given wavelength a perfectly conducting cylinder of radius R possesses $\sigma_T/2R = 2$ in the limit of $R\to\infty$, whereas a perfectly

#130951 - $15.00 USD Received 30 Jun 2010; revised 4 Aug 2010; accepted 5 Aug 2010; published 6 Aug 2010

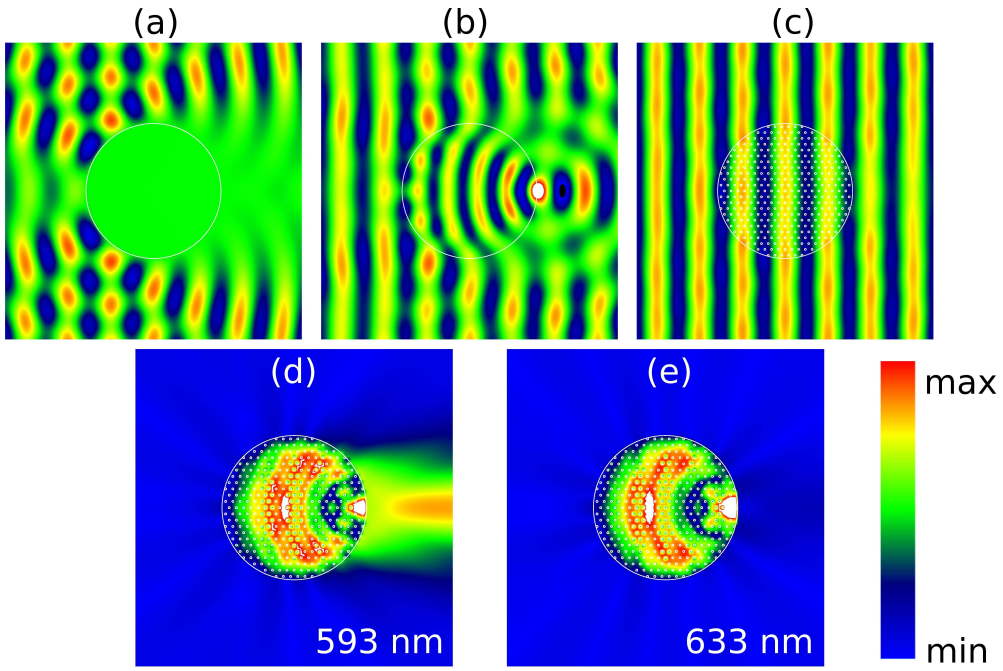

Fig. 5. Electric field (out of plane) at λ = 633nm incident on a R = 1μm (a) silver, (b) silica and (c) metamaterial cylinder. (d) Magnitude of scattered electric field for 1μm metamaterial cylinders at λ = 593nm, where only the impedance is unity, and (e) at λ = 633nm, where only the refractive index is unity.

absorbing cylinder possesses $\sigma_T/2R$ = 1 in the same limit. We refer to the vast literature on the scattering cross section for further details [34].

We calculate σ_T at optical wavelengths for a fibre composed of the metamaterial presented in Section 2.2, formed by 361 hexagonally arranged silver cylinders with radius r = 13.5nm and pitch d = 100nm within a silica cylinder of radius R = 1μm in vacuum. We consider normal incidence, with the electric field parallel to the cylinders (TE polarisation, θ = 90°, δ = 90°). The results are shown in Fig. 4(b): the metamaterial fibre has $\sigma_T/2R$ = −12.6dB at λ = 633nm, corresponding to more than a 97% reduction in shadow when compared to equivalent silver or silica cylinders of the same size. Furthermore, the metamaterial fibre has $\sigma_T/2R$ < 0.1 over a 13nm bandwidth (95% reduction in shadow). Additionally, an effective reduction of σ_T occurs over ~100nm with respect to either of its constituent materials. The inset of Fig. 4(b) presents the normalised total SCS at normal incidence for λ = 633nm, as a function of the azimuthal angle φ, demonstrating −12 ± 0.6 dB reduction of total SCS at all angles. The corresponding contour plot of the electric field at λ = 633nm for these three cylinders is shown in Fig. 5(a)–5(c); the designed fibre indeed appears invisible, exhibiting low scattering and loss.

We also calculate σ_T for the same cylinder possessing an effective ε and μ retrieved in Section 2.2 [Fig. 3(d)], finding excellent agreement with the full multipole calculation [Fig. 4(b)]. The minimum SCS occurs at a wavelength when ***Re(n)*** = 1 (minimum phase change), as opposed to when ***Re(z)*** = 1 (minimum reflection). Thus, the interference due to a phase change through the fibre, due to a small perturbation in ***n***, has a more significant effect on σ_T than a reflection due to a small perturbation in ***z***. This is further illustrated in Fig. 5(d) and 5(e), which compares the scattered electric field magnitude $|\mathbf{E}^S|$ for the metamaterial fibre at λ = 593nm (***Re(z)*** = 1.00, ***Re(n)*** = 1.08) and λ = 633nm (***Re(z)*** = 1.07, ***Re(n)*** = 1.00).

#130951 - $15.00 USD Received 30 Jun 2010; revised 4 Aug 2010; accepted 5 Aug 2010; published 6 Aug 2010

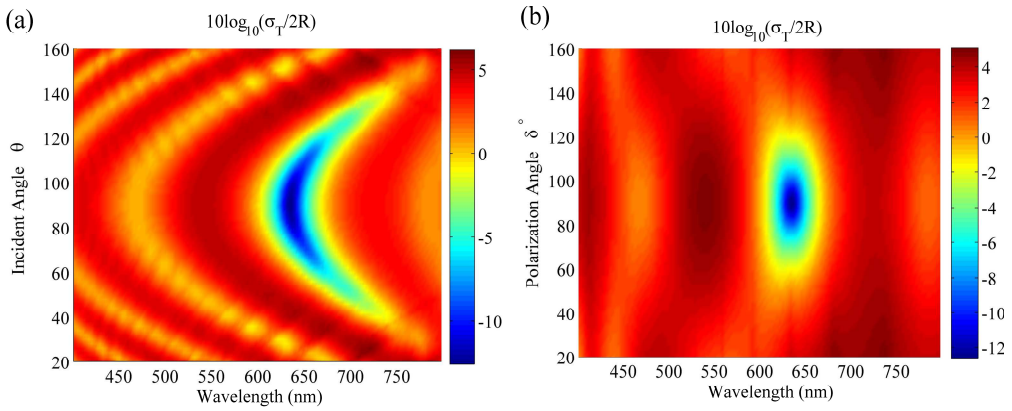

Fig. 6. (a) Colour density plot of normalised SCS as a function of incident angle θ for TE polarisation (δ = 90°), and (b) as a function of polarisation angle δ for normal incidence (θ = 90°).

4. Incident angle, polarisation, and size dependence

We now examine the dependence of σ_T on polarisation and incident angle with respect to the cylinder axis (δ and θ respectively). Thus far we have considered the case δ = 90°, θ = 90°, corresponding to TE polarisation at normal incidence. Figure 6(a) shows a density plot of total scattering cross section as a function of incident angle, while maintaining the polarisation (i.e. we fix δ = 90° and vary θ). Note that σ_T < –10dB for θ = 90 ± 10° with respect to the normal at λ = 633nm. As we increase the incident angle, the regions of minimum scattering move to longer wavelengths, and for θ = 90 ± 50° there exists a wavelength range where $\sigma_T/2R$ < 1 over a bandwidth of ~10nm.

Figure 6(b) shows a density plot of total scattering cross section as a function of polarisation, at constant incident angle (i.e. we fix θ = 90° and vary δ). As expected, the regions of smallest scattering correspond to TE polarisation. As the electric field along the fibre decreases, so does the σ_T. For purely TM polarisation (magnetic field directed along the wires), the cylinder behaves like a dielectric.

In Section 2 we found that the metamaterial used to design our invisible fibre possesses a refractive index of n = 1.00 + 0.01i at λ = 633nm, corresponding to a loss of 0.43dB/μm; achieving a low-loss transparent metamaterial is thus only truly possible at smaller fibre radii. We now examine the influence of metamaterial fibre dimensions on the total scattering cross section.

Figure 7(a) shows the normalised total SCS as a function of R, calculated analytically at λ = 633nm using retrieved optical parameters for the designed metamaterial fibre. As we increase cylinder radius R, $\sigma_T/2R$ reaches unity, thus behaving like a near-perfect absorber. In contrast, the normalised SCS for silver and silica cylinders tends to 2 at large radii, as expected.

Figure 7(b) (crosses) shows the full calculation of the normalised total SCS as a function of R, using the multipole method. The fibres are silica cylinders of radius R centred in the origin, containing silver nanocylinders with r = 13.5nm arranged in a hexagonal array of pitch d = 100nm, such that nanocylinder distance from the origin is $\rho < R\text{-}r$. Since the number of cylinders N increases stepwise with R, the total filling fraction $f_T = Nr^2/R^2$ when increasing R is not constant, and goes through discontinuities. When f_T differs from the ideal value of f, regions at the boundary exist for which the local effective index near the boundary of the metamaterial fibre is not unity, causing increased scattering. Minimal σ_T is thus achieved at values of R for which f_T = 0.659. In particular, we observe the lowest normalised SCS of

#130951 - $15.00 USD Received 30 Jun 2010; revised 4 Aug 2010; accepted 5 Aug 2010; published 6 Aug 2010

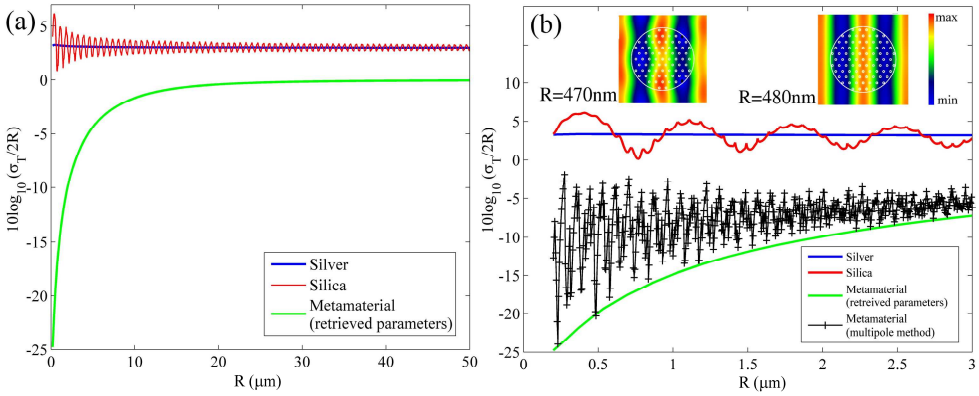

Fig. 7. (a) Analytically computed σ_T at λ = 633nm as a function of cylinder radius, for silver, silica, and our metamaterial cylinder using retrieved parameters. (b) Comparison with full multipole calculation for $R \leq 3\mu m$. Inset: electric field (out of plane) for R = 470nm and R = 480nm.

–24dB for a metamaterial cylinder of R = 230nm. Despite possessing significantly lower SCS compared to silver and silica cylinders of the same size, σ_T is strongly sensitive to total filling fraction, since scattering occurs when the local filling fraction at the metamaterial boundary significantly deviates from that required by design. For example, the inset of Fig. 7 shows a contour plot of the electric field for R = 470nm (containing 73 nanocylinders, thus f_T = 0.602 and $\sigma_T/2R$ = –6.2dB) and R = 480nm (containing 85 nanocylinders, thus f_T = 0.672 and a much reduced normalised total SCS, $\sigma_T/2R$ = –19.4dB).

Note that the metamaterial fibre with R = 3μm already contains 3241 silver nanocylinders. Due to memory constraints, we could not perform a full calculation of the metamaterial total SCS for R > 3μm.

6. Conclusions and future outlook

In conclusion, we have designed and characterised a metamaterial fibre which exhibits a strong reduction in scattering cross section compared to metal and dielectric cylinders of equivalent size. The design procedure can be appropriately adapted to create invisible fibres at any optical wavelength by changing the metal/dielectric filling fraction, or create fibres with other arbitrary permittivity between that of the background and of the metal. Our device operates optimally at the designed wavelength under TE polarisation and normal incidence, yet excellent performance is maintained for ~10nm of bandwidth, or within a ± 10° variation in incident angle with respect to normal incidence, where a reduction in shadow of more than 95% is maintained. Additionally, visibility is significantly reduced over 100nm bandwidth with respect to its constituent materials. Optical parameters obtained from extraction procedures give a good estimate of the total scattering cross section, unless imperfect termination of the nanostructure at the edges causes additional scattering. As with other invisible metamaterials, our device is intrinsically limited by loss, being invisible at small radii, yet behaving like a near-perfect absorber for larger fiber radii. The feasibility of co-drawing metal-dielectric microstructured fibres has already been demonstrated [14,15], and so has the feasibility of drawing air-dielectric nanoscopic features [17]; future work will focus on combining these techniques to produce nanoscale metallic features. While being harder to fabricate, the concept we presented can be extended to produce other 3-dimensional optically invisible structures, such as spheres, which would have a wider tolerance on incident angle and polarisation.

#130951 - $15.00 USD Received 30 Jun 2010; revised 4 Aug 2010; accepted 5 Aug 2010; published 6 Aug 2010

Acknowledgements

This material is based on research sponsored by the Air Force Research Laboratory, under Agreement No. FA2386-09-1-4084. B.T.K. acknowledges support from an Australian Research Council Future Fellowship.

#130951 - $15.00 USD Received 30 Jun 2010; revised 4 Aug 2010; accepted 5 Aug 2010; published 6 Aug 2010

Accepted for publication in Optics Materials Express, to be published in May 2011.

Fiber metamaterials with negative magnetic permeability in the terahertz

Anna Wang,[1,4] Alessandro Tuniz,[1,4*] Peter G. Hunt,[1] Elise M. Pogson,[2] Roger A. Lewis,[2] Avi Bendavid,[3] Simon C. Fleming,[1] Boris T. Kuhlmey[1] and Maryanne C. J. Large[1]

[1]*Institute of Photonics and Optical Science (IPOS), School of Physics, University of Sydney, Sydney, New South Wales 2006, Australia*

[2]*Institute for Superconducting and Electronic Materials, University of Wollongong, Wollongong, New South Wales 2522, Australia*

[3]*Science and Engineering, Commonwealth Scientific and Industrial Research Organization, PO Box 218 Lindfield, Sydney, NSW 2070, Australia*

[4]*These authors contributed equally to this work.*

[*]*alessandro.tuniz@sydney.edu.au*

Abstract: We present a novel method for producing metamaterials with a terahertz magnetic response via fiber drawing, which can be inexpensively scaled up to mass production. We draw a centimeter preform to fiber, spool it, and partially sputter it with metal to produce extended slotted resonators. We characterize metamaterial fiber arrays with different orientations via terahertz time domain spectroscopy, observing distinct magnetic resonances between 0.3 and 0.4 THz, in excellent agreement with simulations. Numerical parameters retrieval techniques confirm that such metamaterials possess negative magnetic permeability. Combined with fiber-based negative permittivity materials, this will enable the development of the first woven negative index materials, as well as the fabrication of magnetic surface plasmon waveguides and subwavelength waveguides.

OCIS codes: (160.2290) Fiber materials; (160.3918) Metamaterials.

References and links

1. N. Fang, H. Lee, C. Sun, and X. Zhang, "Sub-diffraction-limited optical imaging with a silver superlens," Science **308**, 534 (2005).
2. D. Schurig, J. J. Mock, B. J. Justice, S. A. Cummer, J. B. Pendry, A. F. Starr, and D. R. Smith, "Metamaterial electromagnetic cloak at microwave frequencies," Science **314**, 977 (2006).
3. V. M. Shalaev, "Optical negative-index metamaterials," Nat. Photonics **1**, 41-48 (2007).
4. A. Boltasseva, and V. M. Shalaev, "Fabrication of optical negative-index metamaterials: Recent advances and outlook," Metamaterials **2**, 1-17 (2008).
5. J. Hou, D. Bird, A. George, S. Maier, B. T. Kuhlmey, and J. C. Knight, "Metallic mode confinement in microstructured fibres," Opt. Express **16**, 5983-5990 (2008).
6. X. Zhang, Z. Ma, Z. Y. Yuan, and M. Su, "Mass-productions of vertically aligned extremely long metallic micro/nanowires using fiber drawing nanomanufacturing," Adv. Mat. **20**, 1310-1314 (2008).
7. A. Mazhorova, J. F. Gu, A. Dupuis, O. Tsuneyuki, M. Paccianti, R. Morandotti, H. Minamide, M. Tang, Y. Wang, H. Ito, and M. Skorobogatiy, "Composite THz materials using aligned metallic and semiconductor microwires, experiments and interpretation," Opt. Express **18**, 24632-24647 (2010).
8. A. Tuniz, B. T. Kuhlmey, R. Lwin, A. Wang, J. Anthony, R. Leonhardt, and S. C. Fleming, "Drawn metamaterials with plasmonic response at terahertz frequencies," Applied Physics Letters **96**, 191101 (2010).
9. H. K. Tyagi, H. W. Lee, P. Uebel, M. A. Schmidt, N. Joly, M. Scharrer, and P. S. J. Russell, "Plasmon resonances on gold nanowires directly drawn in a step-index fiber," Optics Letters **35**, 2573-2575 (2010).
10. E. Badinter, A. Ioisher, E. Monaico, V. Postolache, and I. M. Tiginyanu, "Exceptional Integration of Metal or Semimetal Nanowires in Human-Hair-Like Glass Fiber," Mat. Lett. **64**, 1902-1904 (2010).
11. J. Du, S. Liu, Z. Lin, and S. T. Chui, "Magnetic resonance of slotted circular cylinder resonators," J. Appl. Phys. **104**, 014907 (2009).
12. C. E. Kriegler, M. S. Rill, M. Thiel, E. Müller, S. Essig, A. Frölich, G. von Freymann, S. Linden, D. Gerthsen, H. Hahn, K. Busch and M. Wegener, "Transition between corrugated metal films and split-ring-resonator arrays," Appl. Phys. B **96**, 749-755 (2009).

13. http://www.zeonex.com
14. R. Singh, E. Smirnova, A. J. Taylor, J. F. O'Hara, and W. Zhang, "Optically thin terahertz metamaterials," Opt. Express **16**, 6537-6543 (2008).
15. M. A. Ordal, R. J. Bell, R. W. Alexander Jr, L. L. Long, and M. R. Querry, "Optical properties of fourteen metals in the infrared and far infrared: Al, Co, Cu, Au, Fe, Pb, Mo, Ni, Pd, Pt, Ag, Ti, V, and W," Appl. Opt. **24**, 4493-4499 (1985).
16. Z. Li, K. Aydin, and E. Ozbay, "Determination of the effective constitutive parameters of bianisotropic metamaterials from reflection and transmission coefficients," Phys. Rev. E **79**, 26610 (2009).
17. N. Katsarakis, T. Koschny, M. Kafesaki, E. N. Economou, and C. M. Soukoulis, "Electric coupling to the magnetic resonance of split ring resonators," Appl. Phys. Lett. **84**, 2943 (2004).
18. C. M. Soukoulis, T. Koschny, J. Zhou, M. Kafesaki, and E. N. Economou, "Magnetic response of split ring resonators at terahertz frequencies," Phys. Stat. Sol. (b) **244**, 1181-1187 (2007).
19. D. Grischkowsky, S. Keiding, M. Exter, and C. Fattinger, "Far-infrared time-domain spectroscopy with terahertz beams of dielectrics and semiconductors," J. Opt. Soc. Am. B **7**, 2006-2015 (1990).
20. E. M. Pogson, R. A. Lewis, M. Koeberle, and R. Jacoby, "Terahertz time-domain spectroscopy of nematic liquid crystals," in Proc. SPIE(2010), p. 77281Y.
21. C. L. Mok, W. G. Chambers, T. J. Parker, and A. E. Costley, "The far-infrared performance and application of free-standing grids wound from 5 μm diameter tungsten wire," Infrared Phys. **19**, 437-442 (1979).
22. T. Koschny, P. Markos, D. R. Smith and C. M. Soukoulis, "Resonant and antiresonant frequency dependence of the effective parameters of metamaterials," Phys. Rev. E **68**, 065602 (2003).
23. L. L. Hou, J. Y. Chin, X. M. Yang, X. Q. Lin, R. Liu, F. Y. Xu, and T. J. Cui, "Advanced parameter retrievals for metamaterial slabs using an inhomogeneous model," J. Appl. Phys. **103**, 064904 (2008). .
24. C. R. Simovski, "On electromagnetic characterization and homogenization of nanostructured metamaterials," J. Opt. **13**, 013001 (2011).
25. L. H. Sperling, *Introduction to physical polymer science* (New York: Wiley-Interscience, 2001).
26. A. Ishikawa, S. Zhang, D. A. Genov, G. Bartal, and X. Zhang, "Deep subwavelength terahertz waveguides using gap magnetic plasmon," Phys. Rev. Lett. **102**, 43904 (2009).

1. Introduction

Metamaterials are artificial materials, composed of sub-wavelength "atoms" that can collectively exhibit effective electromagnetic responses not found in nature. A large number of extraordinary metamaterial devices have been recently reported, e.g. superlenses [1], electromagnetic cloaks [2] and negative refractive index materials [3]. Producing terahertz (THz) and optical metamaterials usually requires expensive and labor-intensive micro- and nano- fabrication processes, such as electron-beam lithography, focused-ion beam milling, nanoimprint lithography and direct laser writing, which limit metamaterial sample sizes to a few centimeters [4]. Here we present a method for the production of a fiber metamaterial possessing negative magnetic permeability, μ, in the THz. Fiber drawing has emerged as means of realizing inexpensive metamaterials, where a macroscopic (centimeter-sized) preform is heated until softened, and drawn into a fiber that is reduced in area by several orders of magnitude and greatly increased in length. Although continuous metal wires down to the micrometer [5-9] and nanometer [10] scale have been reported using such techniques, giving the ability to tailor the effective electric permittivity, ε, this approach has previously never been used for creating magnetically responsive metamaterials.

2. Fabrication and sample preparation

A common approach to produce a negative μ material is to use sub-wavelength metallic split ring resonators (SRRs) composed of a planar open conductive split loop with an inductance L and a capacitance C that opposes incident magnetic fields at frequencies near the LC resonance. The geometry considered here however is the slotted resonator. This has a geometry similar to that of SRRs, but instead of being inscribed in a plane, has a finite depth and is invariant along the longitudinal axis. Slotted resonators can also exhibit a negative magnetic response [11], however their depth demands new fabrication strategies. Recently, slotted resonators in the near- and mid-infrared were produced via a combination of polymer direct-laser writing and chemical vapor deposition [12]. Our approach is to fabricate slotted

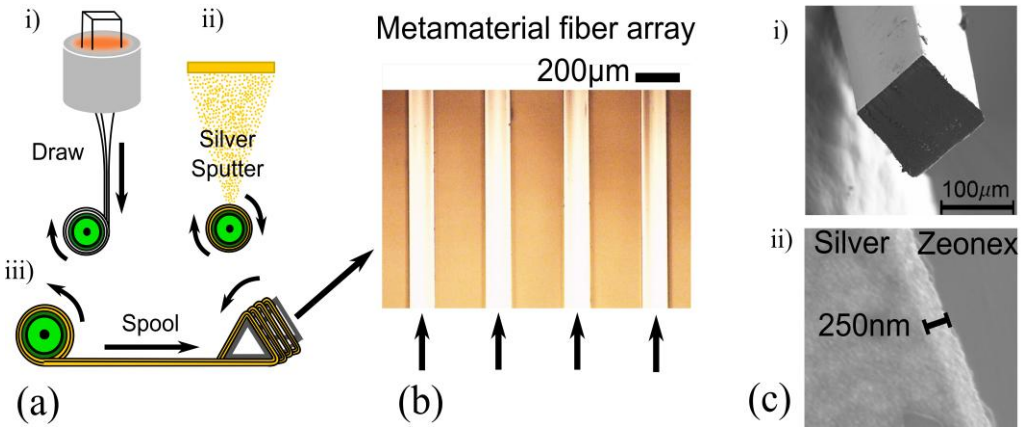

Fig. 1. Schematic of the fabrication procedure. i) A dielectric square preform is drawn, ii) sputtered with silver on three sides and iii) spooled into an array. (b) Optical microscope image of the metamaterial array. (c) SEM micrograph of i) the cross section of the metamaterial fiber and ii) of its 250nm silver coating.

resonators in the fiber form, utilizing the longitudinal uniformity of the fiber drawing process to create kilometers of the required structure.

Figure 1(a) shows a schematic of our fabrication procedure. A preform with a square cross section with 2 cm side was milled from a rod of extruded cyclo-olefin Zeonex [13], a drawable polymer with low loss in the THz region. A square cross-section was chosen to facilitate the spooling of the resulting fiber with a controlled orientation. The preform was drawn to 125±5 μm side, and spooled onto a cylinder which was subsequently loaded in a DC magnetron sputtering deposition system to coat a 200-250 nm silver thin film on three sides.

To ensure the strongest magnetic resonance possible with this geometry [14], the silver coating thickness was selected to be larger than the skin depth δ at 0.1-1 THz. A good approximation of the skin depth for this range of frequencies can be obtained using the d.c. conductivity of silver [15], $\sigma_{dc} = 6\times10^{7}\ \Omega^{-1}m^{-1}$, through $\delta = 1/(f\pi\mu_0\sigma_{dc})^{1/2}$ with μ_0 the permeability of free space and f the frequency at which the skin depth is defined. This yields a skin depth between 50 and 200 nm over the frequency range of interest. To improve adhesion, a chromium interlayer (~10-20 nm) was applied prior to the silver layer deposition. Good silver coating coverage of the three exposed sides was ensured by translating and rotating the spool inside the sputtering chamber [Figure 1(a)]. The resulting fiber formed a single slotted square prism resonator that is invariant along the axis of the fiber. The coated fiber was then spooled again to produce a single flat array, which was supported in a frame [Figure 1(b)]. Figure 1(c) shows a scanning electron microscope (SEM) image of the cross section of our final fiber with 125 μm square edge, and a 250 nm thick silver coating.

By controlling the orientation of the coated fiber at the start of the second spooling process it was possible to produce arrays with different resonator orientations, each with different electromagnetic properties, depending on whether the resonators are symmetric or asymmetric with respect to the forwards- and backwards-propagating wave [16]. Figure 2(c) illustrates the resonator array geometries studied here. In both cases, we consider fields under normal incidence (i.e. propagating in the x-direction), with either the magnetic field (TM polarization) or the electric field (TE polarization) directed along the fiber in the z-direction. In the symmetric case, the resonator will respond isotropically along the x-axis (i.e. the transmission and reflection will be identical whether illumination is from the left or the right), whereas in the asymmetric case it will respond bianisotropically - transmission and reflection will depend on whether the light comes from the left or right. This is due to the lack of inversion symmetry and leads to a magnetoelectric coupling: the magnetic field in z induces an electric dipole in y, and the electric field in y also induces a magnetic dipole in z, in

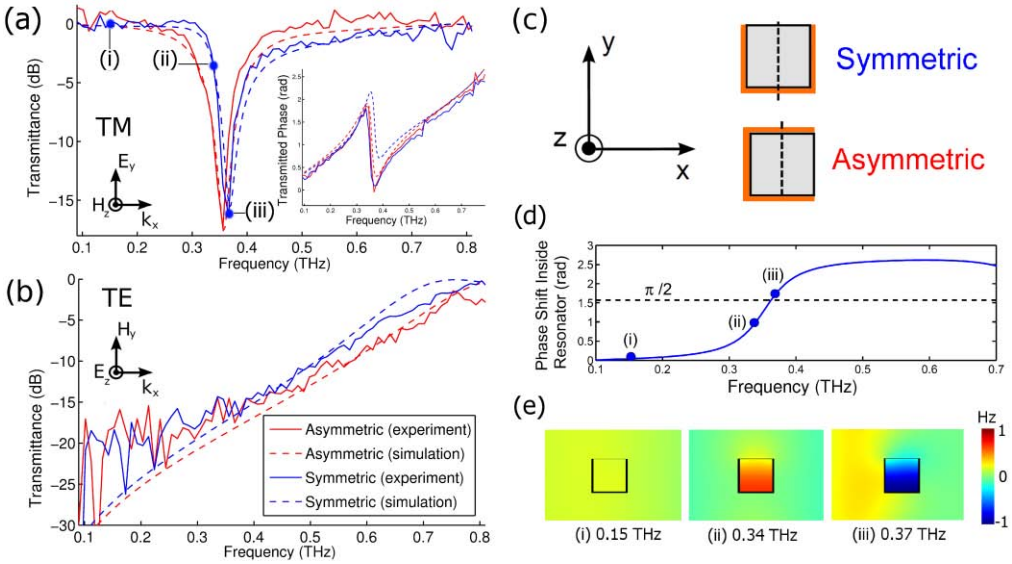

Fig. 2. (a) Experimental and simulated transmittance and phase (inset) under TM polarization. The transmission dip indicates a magnetic resonance. (b) Experimental and simulated transmittance under TE polarization. (c) Schematic of the fiber array orientations. d) Relative phase of the simulated magnetic field at the center of the resonator with respect to the incident field. e) Color plot of the simulated magnetic field incident under TM polarization for the symmetric resonator at (i) 0.15 THz, (ii) 0.34 THz and (iii) 0.37 THz.

particular leading to two different characteristic impedances for two waves propagating in opposite directions [16]. This issue will be considered in the next section, in the context of effective parameter extraction.

Note that in this geometry and for TM incidence, the magnetic field is parallel to the fiber and thus has a nonzero magnetic flux through the resonator loop. By contrast, arrays of thin SRRs are usually printed onto a substrate so that the resonator loops are in the same plane as the array; experimental characterization of one to a few layers of arrays in these cases can only use light normally incident to the substrate as such samples are too thin and would be strongly diffracting in side incidence. The magnetic field is then parallel to the plane of the resonator loops, has zero magnetic flux and is unable to excite a magnetic response. Instead, the electric field is used to generate currents which couple to the magnetic resonance [17] while transmission features due to a magnetic response can be seen in these experiments they do not correspond to a negative permeability [18].

3. Characterization

The transmittance of our samples between 0.1-1 THz was measured experimentally via THz time domain spectroscopy [19, 20]. The transmittance results for the TM and TE waves are shown in Figures 2(a)-(b) for the two fiber orientations. Under TM illumination, our arrays exhibit distinct magnetic resonances between 0.3-0.4 THz, depending on fiber orientation. Under TE illumination, they possess high-pass filtering behavior (without magnetic resonances), analogous to the response of metallic wire-grid structures [21].

We modeled our geometries with the finite element solver COMSOL, using a periodic 2-dimensional array of 125 μm Zeonex squares, coated with a 250 nm silver layer on three sides (using a Drude model [15] for ε) and unit cell size 350 μm. A polynomial fit to experimental data for the refractive index of Zeonex was used in our numerical simulations. There was excellent agreement with experiment in both fiber orientations and polarizations [Figures 2(a)-(b)]. To demonstrate the observed resonances are indeed magnetic, we consider in more detail the fields inside the resonator: Figure 2(d) shows the relative phase of the simulated magnetic

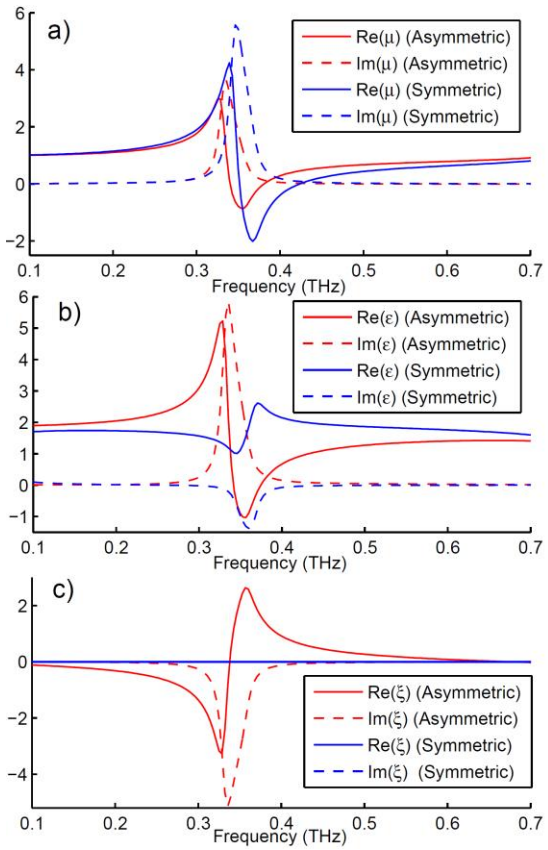

Fig. 4. Real and imaginary parts of the retrieved (a) μ, (b) ε, and (c) magnetoelectric coupling coefficient ξ for the symmetric and asymmetric fiber orientations, under TM polarization. Note that for symmetric resonator orientations ξ is zero.

field at the center of the resonator with respect to the incident field at that point, indicating a near-π phase shift centered around resonance at 0.36 THz. Figure 2(e) shows a color plot of the simulated magnetic field incident under TM polarization for the symmetric resonator (i) far below resonance at 0.15 THz (no magnetic response), (ii) just below resonance at 0.34 THz (in-phase magnetic response) and (iii) just above resonance at 0.37 THz (out-of-phase magnetic response).

We extracted μ and ε of the metamaterial arrays from simulations under TM polarization using the retrieval procedure presented in Ref. [16], taking into account the bianisotropic behavior of our asymmetric fiber array. The complex scattering matrix elements which describe the reflection (S_{11} and S_{22}) and transmission (S_{12} and S_{21}) of the field incident along the x-axis from either side of the array were obtained from the finite element calculations. In the symmetric case there is no magnetoelectric coupling, $S_{11}=S_{22}$ and $S_{12}=S_{21}$; in the asymmetric case however magnetoelectric coupling leads to $S_{11}\neq S_{22}$ and $S_{12}=S_{21}$. Knowledge of the scattering matrix coefficients and metamaterial thickness enable the extraction of the refractive index *n*, from which ε and μ and the magnetoelectric coupling coefficient ξ can be obtained. The results are presented in Figures 3(a)-(c). The symmetric resonator possesses a minimum $\mu = -2+2.2i$ with no magnetoelectric coupling, whereas the asymmetric resonator displays a shallower, red-shifted magnetic response due to magnetoelectric coupling, with a minimum $\mu = -0.9+1.2i$. Correspondingly, ε exhibits antiresonant behavior in the former case, and resonant behavior in the latter [16, 22].

Note that in this work we have measured the transmittance and extracted the effective parameters of a *single* metamaterial layer composed of periodic sub-wavelength resonators. Simulations of single slabs of homogenized material with the extracted ε, μ and ξ indeed reproduce the same transmission and reflection curves as simulations of the full system (not shown). It is known [23] that when considering stacks of *multiple* layers, these parameters differ from the single layer case due to coupling effects between adjacent layers. It follows that the effective ε and μ depend on whether the layer lies inside or on the edge of an arbitrary stack, and effective parameters of stacked layers will also depend on the way layers are stacked (e.g. distance between layers). In such a multiple-layer case, ε and μ can be obtained by analyzing scattering matrices of two- and three- layer systems [23]. Such an analysis becomes relevant in the case of a multi-layer system, and is beyond the scope of this paper. Furthermore, it is important to note that parameters extracted using the above method come from matching of boundary conditions, but do not necessarily reproduce the intrinsic electromagnetic response within the metamaterial [24].

4. Conclusion

In conclusion, we have presented a procedure for making THz metamaterials with a negative effective μ near resonance. The excellent agreement between experiment and simulations demonstrates the very high quality of the fabricated structures. The resonant frequency can be tuned simply by scaling the structure, and can be extended to higher frequencies. Drawing from a preform allows the fabrication of fibers of ~100 μm diameter, however smaller diameters (~10 μm) can be obtained with standard fibers spinning techniques [25], which would move the resonant frequency up to ~10 THz. Further optimization may allow a reduction in size down to 1 μm, allowing the fabrication of resonators into the mid-IR. Whereas for THz resonators the metal thickness is far smaller than the wavelength and surface roughness is not an issue, more care would need to be taken at shorter wavelengths. While in our fabrication setup we use a batch process with a closed sputtering chamber, in-line coating with a continuous operation from preform to metamaterial fiber is possible, with the unique advantage of being able to fabricate metamaterials with a continuous process in very large quantities, literally by the kilometer. Combined with the previously presented fabrication of fiber-based negative ε materials [8] this will enable the development of woven negative index materials, as well as the fabrication of magnetic surface plasmon waveguides and subwavelength waveguides [26]. Advanced weaving techniques will allow the production of materials with gradients of both positive and negative ε and μ, providing the opportunity to demonstrate three dimensional cloaks, as well as hyperlensing from the THz to the mid-IR.

Acknowledgements

This work was performed in part at the Optofab node of the Australian National Fabrication Facility (ANFF) using Commonwealth and NSW State Government funding. ANFF was established under the National Collaborative Research Infrastructure Strategy to provide nano and microfabrication facilities for Australia's researchers. This material is based on research sponsored by the Air Force Research Laboratory, under Agreement No. FA2386-09-1-4084. The work at the University of Wollongong was supported by the Australian Research Council. B.T.K. acknowledges support from an Australian Research Council Future Fellowship. We thank Rainer Leonhardt and Jess Anthony of the University of Auckland for their help in the early stages of this work.